Micromechanical Measurements of Hydrate Particle Attractive Forces

S. Yang[1], D. M. Kleehammer[1], Z. Huo[1], E. D. Sloan,[1] and K. T. Miller[2,C]

Center for Hydrate Research
and
[1]Department of Chemical Engineering
[2]Department of Metallurgical and Materials Engineering

Colorado School of Mines
1500 Illinois St., Golden, CO 80401, USA

[C]Corresponding author:
ktmiller@mines.edu
(Tel.) +1-303-273-3951; (Fax.) +1-303-273-3570

- Properties of Fuels, including Natural Gas Systems

Abstract

Particle-particle pulloff adhesive forces were measured as a function of temperature in the ice/n-decane/ice and THF hydrate/n-decane/THF hydrate systems using a newly developed micromechanical testing technique. Experiments using ~200 μm radius particles were performed at atmospheric pressure over the temperature range 263 - 272 K. While the measured attractive forces had significant scatter, the shapes of the cumulative force distribution curves were similar among the different sets of experiments. The measured pulloff forces distributions shifted to lower force values as the temperature was decreased from the solid melting temperature. The observed forces and trends were explained by the capillary cohesion of rough surfaces, with the capillary bridging liquid being stabilized below its freezing point by the negative curvature of the bridging liquid/n-decane interface.

1. Introduction

The formation of clathrate hydrate plugs in deep-water pipelines is a significant economic and safety concern for the oil and gas industry. At seafloor depths of 1-3 km, the temperature ranges from -2 to 4^{o}C [1], conditions which encourage hydrate formation. Most studies of the kinetics of hydrate formation have focused on particle nucleation and growth [2]. However, hydrate particle aggregation also plays an important role in pipeline plug formation. In pipelines, hydrate particles are expected to nucleate and grow as a film along the water-oil interface; after breakup of this film, dispersed hydrate particles agglomerate, increasing the hydrate suspension viscosity and eventually forming a hydrate plug [3,4].

Hydrate nucleation and growth depend upon well characterized thermodynamic properties, such as equilibrium temperature, pressure, and composition. Aggregation and subsequent rheological behavior, in contrast, depend upon physical and mechanical properties, such as fluid shear rate, particle size, and the interparticle adhesive force. In particular, understanding of the adhesive forces between hydrate particles is poorly developed. Based upon rheological measurements of hydrate/water/crude oil emulsions, Camargo and Palermo [5] speculated that capillary attractions dominate hydrate agglomeration in the oil phase and that subsequent freezing of these necks strengthens the hydrate plug; these hypotheses, however, have not been verified experimentally.

Colloidal interaction forces are typically measured using either the surface forces apparatus [6-8] or colloidal probe atomic force microscopy [9-12]. Difficulties in sample preparation, however, make these techniques poorly suited to measurements of clathrate hydrate and ice particle adhesive forces. Moreover, neither of these techniques is capable of directly examining the particle-particle adhesive interactions which determine aggregated suspension rheological behavior. In contrast, a recently developed micromechanical testing technique [13,14] can be used to directly measure particle-particle pulloff forces [14]. This technique uses digital video microscopy to track the movement of particles attached to low spring constant ($\geq 10^{-2}$ N/m) cantilever beams, as the beams are displaced with micromanipulators. In this paper, we adapt this technique to the measurement of particle-particle pulloff forces in ice and clathrate hydrates. Specifically, we examine, as a function of temperature, the pulloff forces between particles in the (1) ice/n-decane/ice and (2) THF hydrate/n-decane/THF hydrate systems. We then compare the measured forces to those expected for van der Waals attraction and capillary adhesion.

2. Experimental Procedure

The micromechanical measurement technique [14] is illustrated schematically in Figure 1. In this method, ice or hydrate particles are attached to the ends of glass fiber cantilevers using a droplet quenching technique described in more detail below. The glass fiber cantilevers in turn are held by micromanipulators under an inverted light microscope (Carl Zeiss Axiovert S100). A low precision hand-operated micromanipulator (Narishige MN-151) is used to position one of the particles in the microscope's field of view. The base of this cantilever is held stationary during the experiment. Using a high precision remote-operated micromanipulator (Eppendorf Patchman 5173), a second particle is brought into contact with the first, held stationary for several seconds, and then gently pulled away. Since the particles adhere, the stationary cantilever bends. At a critical force, the adhesive bond breaks and the particles quickly pull apart. Video of this entire process was recorded using a grayscale 1/2" CCD camera (Cohu, Model 4915-2030) and was directly digitized using a framegrabber card (Scion, LG3) in a personal computer. The cantilever displacement at particle separation was determined using the public domain image analysis programs NIH Image and ImageJ (developed at the U. S. National Institute of Health and available at *http://rsb.info.nih.gov/nih-image*); an example of this is shown in Figure 2.

The pulloff force F is determined from the displacement δ using through the spring constant k of the cantilever beam,

$$F = k\,\delta \tag{1}$$

For the cylindrical fibers used in this apparatus, k can be determined from the fiber dimensions through the relation

$$k = \frac{3\pi E d^4}{64 L^3} \tag{2}$$

where E is the elastic modulus of the glass and d and L are the fiber diameter and length. The glass fibers used in this study had an elastic modulus of 70 GPa, and diameters and lengths of approximately 27 µm and 3.5 mm, respectively, giving spring constants of

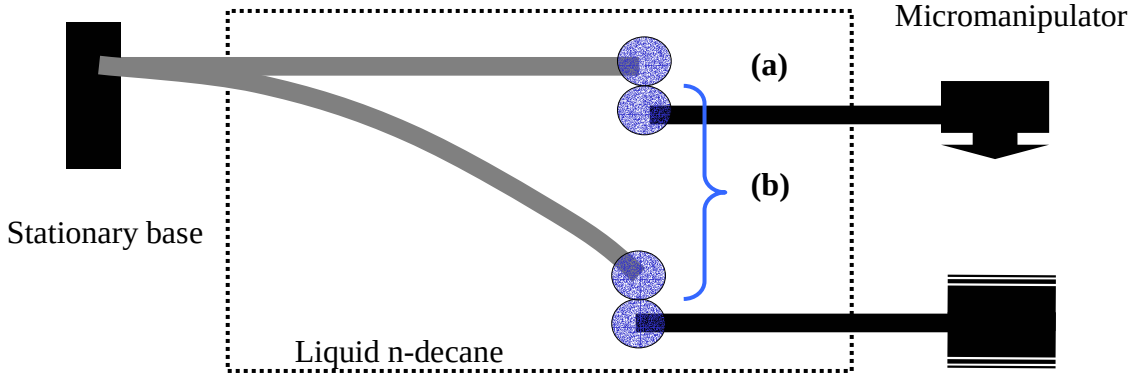

Figure 1. Schematic illustration of the micromechanical testing apparatus.

~0.15 N/m. The diameter and length of each cantilever were determined individually from microscopic measurements; additional experiments showed that the spring constants determined from fiber dimensions were within 10% of those determined by a dead loading method.

Ice and tetrahydrofuran (THF) hydrates were used in this study. To prepare the sample, a liquid droplet of either water or aqueous THF solution was placed at the end of the cantilever. This droplet was then rapidly solidified by either quenching in liquid N_2 or placing the droplet near solid CO_2. Because THF is highly volatile, slightly THF-rich solutions were used; the stoichiometric THF hydrate composition is H_2O (19.07 wt% THF), while H_2O (20 wt% THF) solutions were typically used in this study. Particles prepared with this technique had a radius of approximately 200 µm.

All experiments were performed under ambient pressure. For low temperature control, a custom-made liquid cooling stage was installed on the microscope. In this stage, an outer jacket of circulating water-ethylene glycol solution was used to cool an inner chamber of quiescent n-decane. The coolant temperature was maintained within ±0.2 K, which resulted in an inner chamber temperature control of ±0.5 K. In these experiments, the temperature of the n-decane liquid was varied from -10 to 2 °C. After quenching, the particles were rapidly installed in the cooling stage to avoid evaporation and melting.

3. Results

Over 950 individual pulloff measurements were performed, in 28 sets of unique combinations of temperature and pairs of particles. While the droplet quenching technique typically produced particles with a radius of approximately 200 µm, there was some variability in this value, with the radius of the ice particles varying from 115 - 248 µm and the hydrate particles from 159 - 271 µm. To directly compare the pulloff force results from

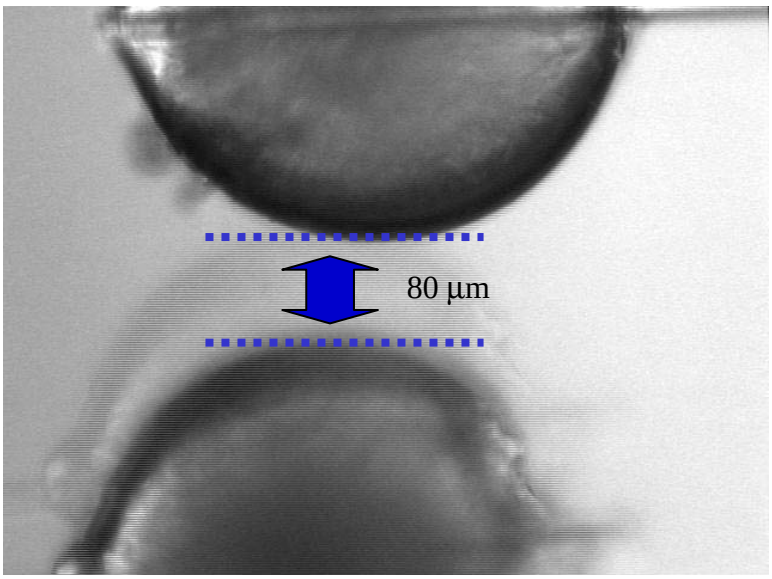

Figure 2. Displacement of hydrate particles at pulloff.

different particle pairs, all force measurements were normalized by the harmonic mean radius of the particle pair, R^*, where

$$\frac{1}{R^*} = \frac{1}{2}\left(\frac{1}{R_1} + \frac{1}{R_2}\right) \tag{3}$$

and R_1 and R_2 are the radii of the first and second particles. For the ice particles, $R^* = 185 \pm 35$ µm, and for the hydrate particles, $R^* = 212 \pm 15$ µm.

The measured pulloff forces showed considerable scatter. Figure 3 shows a typical cumulative force distribution curve, in this case for ice particles at -4.8 °C. The pulloff force distribution typically has a minimum value near zero (occasionally the particles do not measurably adhere after contact) and a "tail" at relatively large forces, with many of the data sets appearing to follow a log-normal distribution. The shapes of the distributions are also similar across the data sets. For example, Figure 4 shows that the maximum force measured in each set is approximately 3.1 times the median force. The individual measurements in each data set, however, are not correlated; the force measured in one contact does not predict the subsequently measured forces, and the force does not systematically increase or decrease with the number of contacts.

In both the ice and hydrate experiments, the median and maximum forces increased with increasing temperature. Figure 5 shows the force distributions for a single pair of hydrate particles which were tested in a series of increasing temperatures. The distributions are clearly shifted toward greater force as the temperature is increased toward the hydrate melting temperature (4.4 °C). The maximum measured force in each distribution is plotted as a function of temperature for the hydrate and ice particles in Figures 6 and 7.

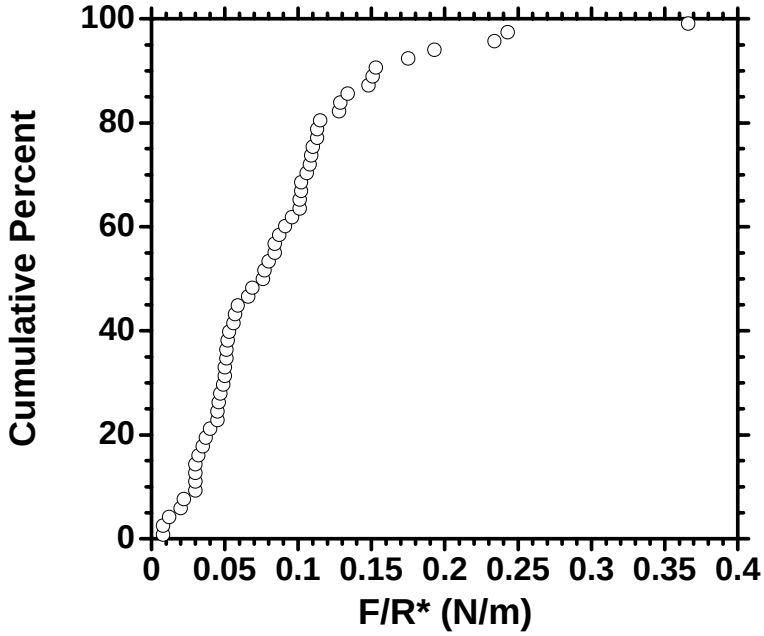

Figure 3. Cumulative force distribution curve for ice particles at -4.8 °C.

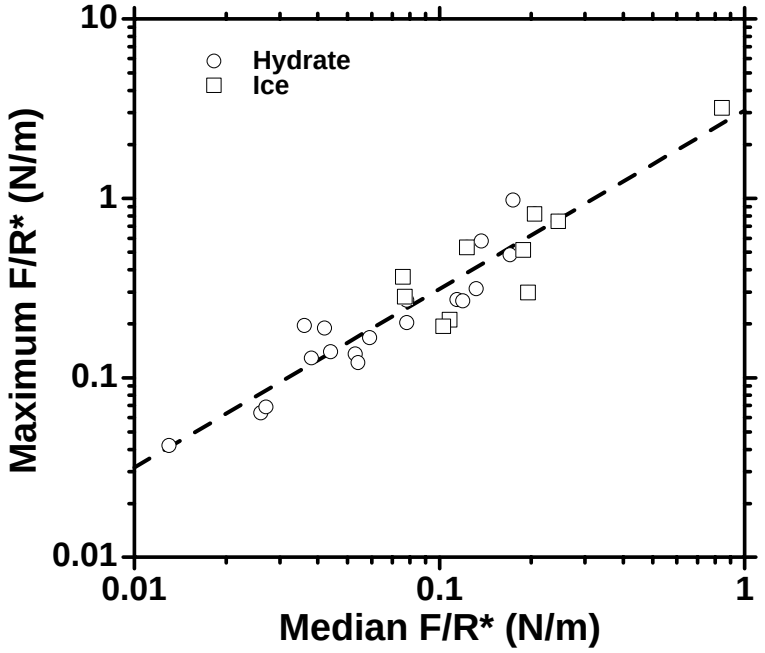

Figure 4. Maximum value of each force distribution set, as a function of the median of the set.

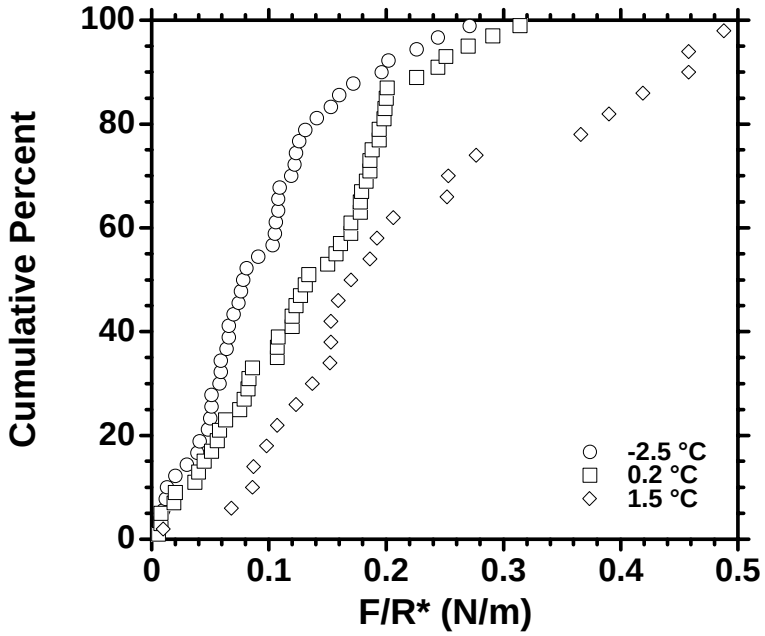

Figure 5. Cumulative force distributions for a single pair of hydrate particles as a function of increasing temperature.

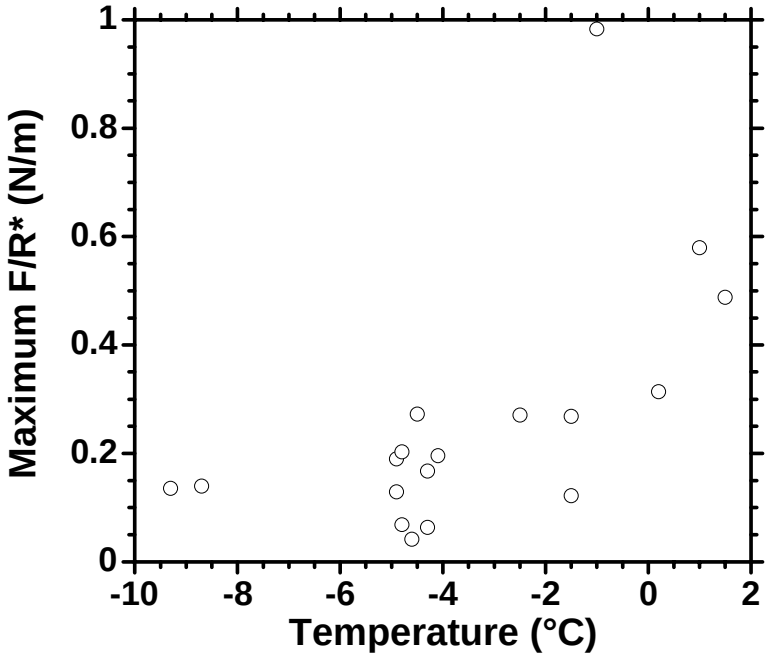

Figure 6. Maximum hydrate pulloff force in each data set, as a function of temperature.

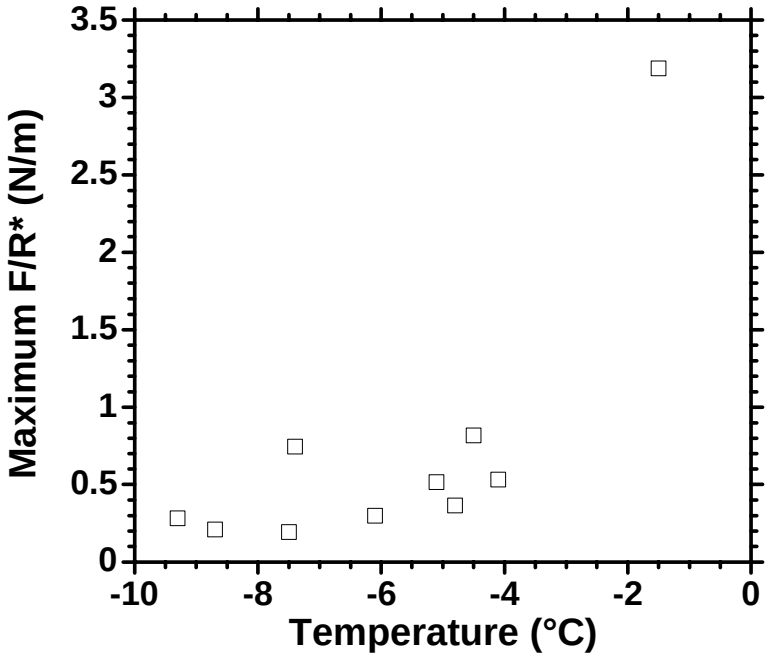

Figure 7. Maximum ice pulloff force in each data set, as a function of temperature.

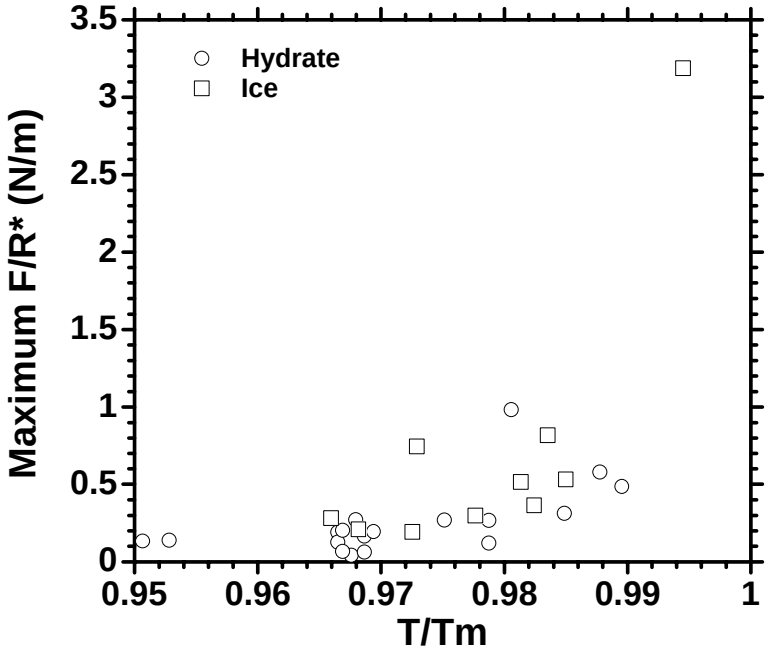

Figure 8. Maximum of each force distribution data set, as a function of normalized temperature.

Similar curves could be generated for the median and average forces. While there is considerable scatter in the data, there is clearly a trend of increasing pulloff force as temperature is increased toward the melting point of the material. The shapes of the two curves are also very similar. When normalized by the melting temperature of the solid phase (0 °C for ice, 4.4 °C for THF hydrate), the curves overlap, as seen in Figure 8. This suggests a common mechanism which depends upon the melting temperature of the solid.

4. Discussion

Three possible causes for observed adherence of the particles are (1) sintering of the particles, (2) van der Waals attraction, or (3) capillary bridges of water at the particle necks. Sintering is unlikely for two reasons. First, the particles were in contact for only a few seconds, and, in limited experiments, the pulloff force was not observed to increase with contact time. Second, the particle surfaces were sometimes observed to slide before pulloff, which would break any newly-developed necks.

The observed pulloff forces are also much larger than could be attributed to the van der Waals attraction. At close interparticle distances, the van der Waals force F_A between two spheres is given by [15]

$$\frac{F_A}{R^*} = \frac{A}{12\,H^2} \tag{4}$$

where A is the Hamaker constant, H is the distance of closest approach between the particle surfaces, and R^* is the harmonic mean radius given by Eq. (3). From known refractive indices, Camargo and Palermo [5] estimated the Hamaker constant for hydrates across alkanes to be 5.0 x 10^{-21} J. Taking 0.25 N/m as a typical measured value of F/R^* in our system, Eq. (4) implies an interparticle distance of 0.4 Å, clearly an unphysically small value.

In contrast, capillary bridge forces are the proper magnitude to explain the measured pulloff forces. Considering only the attractive force from the Laplace pressure of the capillary liquid, the simple equilibrium model for a capillary bridge pulloff [15] shows that the force is given by

$$\frac{F_B}{R^*} = 2\pi \gamma_{LL} \cos\theta \tag{5}$$

where γ_{LL} is the liquid-liquid interfacial energy and θ is the contact angle of the capillary liquid on the solid particle. The contact angle of water on either hydrate or ice is expected to be 0° due to the strongly hydrophilic nature of the surfaces. Estimating the energy of the n-decane/water interface to be 50 mN/m [15] yields a value of F_B/R^* of 0.31 N/m. The measured forces are of this magnitude, strongly suggesting a capillary bridging mechanism. (Exact agreement should not be expected because of the simplicity of the model and the nonequilibrium nature of the capillary bridge during the pulloff experiment.)

The capillary bridging mechanism also explains the highly variable nature of the hydrate pulloff experiments. In laboratory conditions, hydrates nucleate and grow at the gas-water interface, producing a rough surface [16]. When rough surfaces contact, capillary bridges between the surfaces may only fill in some of the asperities [15,17], producing a wide variety of bridging area from one pulloff measurement to the next.

On first consideration, the presence of liquid capillary bridges at temperatures below the aqueous freezing point (4.4 °C for THF hydrate, 0 °C for ice) seems counterintuitive. Recall, however, that the chemical potential of liquid beneath a curved interface, such as that found at a capillary bridge, is lowered from that of a flat interface according to the Laplace equation,

$$\Delta\mu = \frac{2\gamma_{LL} V_m}{r^*} \tag{6}$$

where V_m is the molar volume of the bridging liquid and r^* is the harmonic mean curvature of the interface. This is determined from the two principle radii of curvature, r_1 and r_2,

$$\frac{1}{r^*} = \frac{1}{2}\left(\frac{1}{r_1} + \frac{1}{r_2}\right) \tag{7}$$

The lowered chemical potential of the capillary bridge stabilizes the liquid phase, and allows liquid water or THF solution to exist below the equilibrium freezing point. Figure 9 shows, as a function of temperature, the minimum value of the liquid radius of curvature

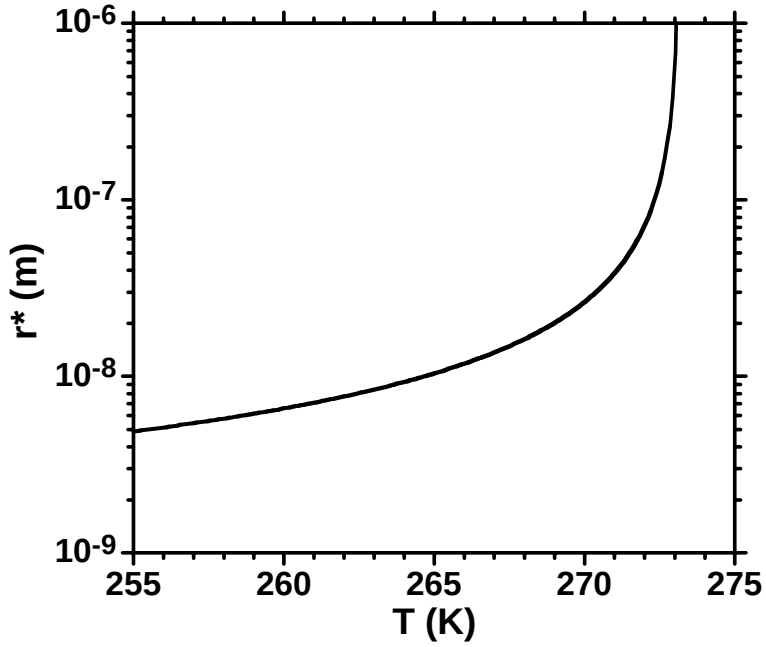

Figure 9. Negative harmonic mean curvature *r** required to stabilize liquid water, as a function of temperature.

which is required to stabilize pure liquid water. In this calculation, the free energy difference between solid and liquid water under a flat interface was calculated as a function of temperature using the standard thermodynamic properties of water. This energy difference was then set equal to the chemical potential difference between the curved and flat interfaces (Eq. 6), and *r** (which has a negative value) was determined. For the undercoolings in the current experiments, *r** has a minimum value of ~6 nm, which is reasonable when compared to values from capillary condensation.

The decrease in pulloff force with decreasing temperature can be explained by the combined effects of surface roughness and curvature stabilization of the bridging liquid. As the temperature decreases, the radii of curvature must decrease to maintain stabilization of the liquid phase (Figure 9). If the surface is rough compared to the scale of the bridging liquid radius of curvature, only some of the potential contact area of the particles will be bridged. (This is analogous to the decrease in pulloff force with decreasing relative humidity which is observed in capillary condensation between rough surfaces [15].) The bridged area, and thus the pulloff force, should therefore decrease with decreasing temperature. This is the trend that is observed in the current experiments.

Conclusions

Adhesive pulloff forces have been measured for particle pairs in the ice/n-decane/ice and THF hydrate/n-decane/ THF hydrate systems. The measured attractive forces showed a large degree of scatter, but the shapes of the cumulative force distribution curves were similar among the different series of experiments. The measured forces also decreased as

the temperature was lowered from the freezing point of the particles. The observed forces and trends were explained by the capillary cohesion of rough surfaces, with the capillary bridging liquid being stabilized below its freezing point by the negative curvature of the bridging liquid/n-decane interface.

Acknowledgements

This work was supported by the Colorado School of Mines Center for Hydrate Research, a research consortium funded by BP, ChevronTexaco, ExxonMobile, Haliburton, Philips Conoco, and Unocal. The development of the micromechanical testing apparatus was funded by the National Science Foundation, under CAREER Award #9876135. The authors would also like to thank Graham Mustoe, Doug Turner, and Lennart Bergström for helpful discussions.

References

1. J. S. Gudmundsson, "Cold Flow Technology," p. 912-916 in *Proceedings of the 4th International Hydrates Conference*, Yokohama, Japan (2002).
2. J. -M. Herri, J. S. Pic, F. Gruy and M. Cournil, "Methane Hydrate Crystallization Mechanism from In-Situ Particle Sizing", *AIChE J.*, **45** [3] 590-602 (1999).
3. T. Ausvik, L. Xiaoyun, and L. H. Gjertsen, "Hydrate Plug Properties: Formation and Removal of Plugs," p. 294-303 in *Proceedings of the 3rd International Hydrates Conference*, Salt Lake City, Utah (1999).
4. M. N. Lingelem, A. I. Majeedm, and E. Stange, "Industrial Experience in Evaluation of Hydrate Formation, Inhibition, and Dissociation in Pipeline Design and Operation," *Proceedings of the 1st International Hydrates Conference*, New-Paltz, New York (1993).
5. R. Camargo and T. Palermo, "Rheological Properties of Hydrate Suspension in an Asphaltenic Crude Oil," p. 880-885 in *Proceedings of the 4th International Hydrates Conference*, Yokohama, Japan (2002).
6. D. Tabor and R. H. S. Winterton, "The Direct Measurement of Normal and Retarded Van Der Waals Forces," *Proc. R. Soc. London, Ser. A*, **312**, 435-450 (1969).
7. J. N. Israelachvili and G. E. Adams, "Measurement of Forces between Two Mica Surfaces in Aqueous Electrolyte Solutions in the Range of 0-100 nm," *J. Chem. Soc., Faraday Trans. 1*, **74**, 975-1001 (1978).
8. G. Vigil, Z. Xu, S. Steinberg, and J. Israelachvili, "Interactions of Silica Surfaces," *J. Colloid Interface Sci.*, **165**, 367-385 (1994).
9. W. A. Ducker, T. J. Senden, and R. M. Pashley, "Direct Measurement of Colloidal Forces Using an Atomic Force Microscope," *Nature*, **353**, 239-241 (1991).
10. W. A. Ducker and T. J. Senden, "Measurement of Forces in Liquids Using a Force Microscope," *Langmuir*, **8** [7] 1831-1836 (1992).

11. H.-J. Butt, M. Jaschke, and W. Ducker, “Measuring Surface Forces in Aqueous Electrolyte Solution with the Atomic Force Microscope,” *Biochem. Bioenerg.*, **38** [1] 191 (1995).

12. I. Larson, C. J. Drummond, D. Y. C. Chan, and F. Grieser, “Direct Force Measurements Between Silica and Alumina,” *Langmuir*, **13** [7] 2109-2112 (1997).

13. A. K. C. Yeung and R. Pelton, “Micromechanics: A New Approach to Studying the Strength and Breakup of Flocs,” *J. Colloid Interface Sci.*, **184**, 579-585 (1996).

14. K. L. Eccleston and K. T. Miller, “Direct Measurement of Strongly Attractive Particle-Particle Interactions,” p. 33-36 in *Improved Ceramics through New Measurements, Processing, and Standards (Ceramic Transactions Volume 133),* edited by M. Matsui, S. Jahanmir, H. Mostaghaci, M. Naito, K. Uematsu, R. Wäsche, and R. Morrell, American Ceramic Society (2002).

15. J. N. Israelachvili, *Intermolecular and Surface Forces, 2nd Ed.*, Academic Press, London (1992).

16. P. Servio and P. Englezos, “Morphology of Methane and Carbon Dioxide Hydrates Formed from Water Droplets,” *AIChE J.*, **49** [1] 269-276 (2003).

17. E. R. Beach, G. W. Tormoen, J. Drelich, and R. Han, “Pull-off Measurements Between Rough Surfaces by Atomic Force Microscopy,” *J. Colloid Interface Sci.*, **247**, 87-99 (2002).